

RESEARCH ARTICLE

[View Article Online](#)  
[View Journal](#) | [View Issue](#)



Cite this: *Inorg. Chem. Front.*, 2023, **10**, 6407

## A highly connected metal–organic framework with a specific nonpolar nanotrap for inverse ethane/ethylene separation†

Jing-Jing Pang,<sup>a</sup> Zhi-Han Ma,<sup>a</sup> Qiang-Qiang Yang,<sup>a</sup> Kuo Zhang,<sup>a</sup> Xin Lian,<sup>a</sup> Hongliang Huang,<sup>ID \*b</sup> Zhao-Quan Yao,<sup>\*c</sup> Baiyan Li,<sup>ID</sup><sup>a</sup> Jian Xu <sup>ID \*a</sup> and Xian-He Bu <sup>ID a,d</sup>

Efficient separation of ethylene ( $C_2H_4$ ) from ethane ( $C_2H_6$ ) via a one-step adsorption process is desirable yet challenging. In this work, we report a  $C_2H_6$ -selective polynuclear  $Tb$ -MOF  $[Tb_9(\mu_3-O)_2(\mu_3-OH)_{12}(H_2O)_9(TCPE)_3]^- \cdot [H_3O]^+ \cdot (\text{solvents})_x$  ( $TCPE = \text{tetrakis}(4\text{-carboxyphenyl})\text{ethylene acid}$ ), **NKU-200-Tb**, assembled via the reticular chemistry principle. The resulting (4,12)-connected framework critically features a high density of nonpolar aromatic rings on the pore surface and forms a specific nanotrap for  $C_2H_6$  with multiple  $C-H \cdots \pi$  interaction sites. As a result, **NKU-200-Tb** exhibits an inverse adsorption behavior with a high  $C_2H_6/C_2H_4$  selectivity of 2.06 and a large uptake ratio of 151% ( $60.27/39.95 \text{ cm}^3 \text{ g}^{-1}$ ) at 298 K and 1 bar. The superior adsorption properties of **NKU-200-Tb**, combined with great structural stability, place it among the most promising stable  $C_2H_6$ -selective MOFs. Dynamic breakthrough experiments demonstrate that polymer-grade  $C_2H_4$  (>99.9%) can be harvested in one step from a binary mixture of  $C_2H_6/C_2H_4$  (10/90, v/v). This work signifies the synergy of pore surface chemistry and space confinement in promoting the challenging  $C_2H_6/C_2H_4$  separation.

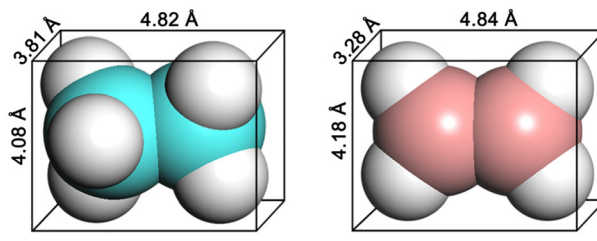
Received 13th August 2023,  
Accepted 13th September 2023

DOI: 10.1039/d3qi01595e

rsc.li/frontiers-inorganic

Ethylene ( $C_2H_4$ ) is one of the most important chemical feedstocks in the petrochemical industry due to its wide use in the manufacture of polymers, plastics, polyesters, and other commodity chemicals, wherein polymer-grade  $C_2H_4$  (>99.9% pure) is required.<sup>1</sup> However, the crude olefin products obtained through the cracking of naphtha inevitably contain a small amount of ethane ( $C_2H_6$ ) impurity, and their separation is presently considered as the most challenging industrial separation ascribed to their very similar molecular dimensions and physicochemical properties (Scheme 1).<sup>2</sup> Cryogenic distillation technology is the prevalent solution in industry for separating  $C_2H_4$  from  $C_2H_6$ , which is usually operated in a large distillation tower (120–180 trays) at low temperatures (180–258 K) and

high pressures (5–28 bar), thereby coming with a high energy penalty.<sup>3</sup> As far as is known, purification of olefin (*i.e.*, ethylene and propylene) from paraffin (*i.e.*, ethane and propane) accounts for 0.3% of global energy use and has been regarded as one of the “seven chemical separations to change the world”.<sup>4</sup> Thus, developing an alternative method of purifying



	KD (Å)	BP (K)	Polarizability ( $10^{-25} \text{ cm}^3$ )	QM ( $10^{-26} \text{ esu cm}^3$ )
$C_2H_6$	4.4	184.6	44.3	0.65
$C_2H_4$	4.2	169.5	42.5	1.50

**Scheme 1** Molecular structure and physical properties of  $C_2H_6$  and  $C_2H_4$ . KD = kinetic diameter. BP = boiling point, QM = quadrupole moment.

<sup>a</sup>School of Materials Science and Engineering, Smart Sensing Interdisciplinary Science Center, TKL of Metal and Molecule-Based Material Chemistry, Nankai University, Tianjin 300350, China. E-mail: jxu@nankai.edu.cn

<sup>b</sup>School of Chemistry and Chemical Engineering, Tiangong University, Tianjin 300387, China. E-mail: huanghongliang@tiangong.edu.cn

<sup>c</sup>School of Chemistry and Chemical Engineering, Tianjin University of Technology, Tianjin, 300384, China. E-mail: yaoqz@email.tjut.edu.cn

<sup>d</sup>State Key Laboratory of Elemento-Organic Chemistry, Frontiers Science Center for New Organic Matter, Collaborative Innovation Center of Chemical Science and Engineering (Tianjin), Nankai University, Tianjin 300071, China

† Electronic supplementary information (ESI) available: Additional crystallographic and magnetic data. See DOI: <https://doi.org/10.1039/d3qi01595e>

$\text{C}_2\text{H}_4$  in an energy-efficient manner is urgently desirable and essential to reduce energy footprint.

Adsorptive separation by porous materials has emerged as a promising technology for addressing olefin purification.<sup>5,6</sup> In this regard, metal-organic frameworks (MOFs) have great advantages over conventional porous solids (e.g., zeolites, activated carbon, and mesoporous silica) in terms of gas adsorption selectivity and capacity, on account of their programmable pore structures and customizable pore environments.<sup>7,8</sup> Over the past decade, many MOF adsorbents have been designedly constructed and shown preferential adsorption of  $\text{C}_2\text{H}_4$  over  $\text{C}_2\text{H}_6$ , relying on molecular sieving,<sup>9,10</sup>  $\pi$ -complexation,<sup>11</sup> or electrostatic interaction between the  $\pi$ -clouds of olefin and highly polar groups (e.g., open metal sites).<sup>12</sup> In order to obtain polymer-grade ethylene, these  $\text{C}_2\text{H}_4$ -selective adsorbents have to be subjected to multiple adsorption–desorption cycles to remove the co-adsorbed impurity, inevitably involving energy-intensive desorption and regeneration steps by temperature or vacuum swing.<sup>13</sup> In contrast, the adsorbents with inverse adsorption selectivity for  $\text{C}_2\text{H}_6$  over  $\text{C}_2\text{H}_4$  can harvest pure  $\text{C}_2\text{H}_4$  directly at the outlet through a single-step adsorption process with about 40% energy saving.<sup>14–17</sup> However, such  $\text{C}_2\text{H}_6$ -selective adsorbents reported to date are much fewer than the  $\text{C}_2\text{H}_4$ -selective ones probably due to two major reasons: first, the kinetically driven separation or molecular sieving is inaccessible for achieving inverse adsorption behavior in rigid MOFs, as the kinetic diameter of  $\text{C}_2\text{H}_6$  is larger than that of  $\text{C}_2\text{H}_4$ . Second, there is a lack of suitable strong paraffin affinity sites compared with olefin, bringing difficulty in designing delicate pore environments to trap  $\text{C}_2\text{H}_6$ .

In recent five years, significant efforts have been dedicated to the construction of non-trivial paraffin-selective MOFs and gained much progress.<sup>18</sup> Among the proposed design strategies, the most sophisticated one is to customize an inert/hydrophobic pore surface composed of nonpolar aromatic rings or aliphatic chains in the absence of open metal sites, which is envisaged to attain more nonspecific van de Waals (vdW) interactions with  $\text{C}_2\text{H}_6$  due to its larger polarizability than  $\text{C}_2\text{H}_4$  ( $44.3 \times 10^{-25} \text{ cm}^3$  vs.  $42.5 \times 10^{-25} \text{ cm}^3$ ) and more C–H binding sites.<sup>19</sup> With this principle, a series of  $\text{C}_2\text{H}_6$ -selective MOFs have been successfully fabricated,<sup>20–23</sup> but many of them suffer from insufficient  $\text{C}_2\text{H}_6/\text{C}_2\text{H}_4$  selectivity (<2) partly due to the relatively weak interaction nature of vdW forces. One straightforward way to overcome this dilemma is increasing the number of such vdW interactions by promoting the density of functional affinity sites or enhancing confinement to enlarge the contact area of the pore surface with gas molecules, both of which are, however, still underexplored. In addition to adsorption properties, the structural stability of adsorbents should also be considered. For example,  $\text{Fe}_2(\text{O}_2)$  (dobdc) with a record  $\text{C}_2\text{H}_6/\text{C}_2\text{H}_4$  selectivity has to be operated in a glove box because of its poor stability in environments,<sup>15</sup> greatly hindering its industrial application.

Bearing these in mind, we sought to explore the adsorption and separation performance of a (4,12)-connected Tb-MOF, namely **NKU-200-Tb**,<sup>24</sup> based on a nonanuclear  $\text{Tb}_9$  node and

the aromatic linker tetrakis(4-carboxyphenyl)ethylene acid ( $\text{H}_4\text{TCPE}$ , Fig. S1 and S2†), due to the following considerations. First, its highly connected **shp** network constitutes a large  $\pi$ -conjugated system enriched with nonpolar aromatic rings, promoting the density of functional affinity sites for  $\text{C}_2\text{H}_6$ . Second, its framework contains three types of channels with different shapes and apertures, holding high promise to offer suitable confinement and multi-site adsorption for  $\text{C}_2\text{H}_6$ . Third, the high connectivity of the framework and the strong coordination bond between the  $\text{Tb}^{3+}$  ion (hard Lewis acid) and carboxylate ligand (hard Lewis base) endow it with excellent structural stability. In line with the above analyses, **NKU-200-Tb** shows the desired inverse adsorption behavior with a high  $\text{C}_2\text{H}_6/\text{C}_2\text{H}_4$  selectivity of 2.06 at 298 K and 1 bar, surpassing many reported  $\text{C}_2\text{H}_6$ -selective MOFs. Further density functional theory (DFT) calculations disclose that the aperture window of one channel with suitable pore size forms a nanotrap to promote the  $\text{C}_2\text{H}_6/\text{C}_2\text{H}_4$  separation by the enhanced confinement. As a result, **NKU-200-Tb** achieves a good performance for purifying  $\text{C}_2\text{H}_4$  (>99.9%) in one step from a binary mixture of  $\text{C}_2\text{H}_6/\text{C}_2\text{H}_4$  (10/90, v/v), as demonstrated by breakthrough experiments, placing it among the promising one-step  $\text{C}_2\text{H}_4$  purification adsorbents.

The crystalline **NKU-200-Tb** was synthesized according to our previous report.<sup>24</sup> Single-crystal X-ray diffraction analysis reveals that it crystallizes in the trigonal space group  $P\bar{3}$  with the formula  $[\text{Tb}_9(\mu_3\text{O})_2(\mu_3\text{-OH})_{12}(\text{H}_2\text{O})_9(\text{TCPE})_3]^- \cdot [\text{H}_3\text{O}]^+ \cdot (\text{solvents})_x$  (Fig. S3 and Table S1†). In this structure, the nonanuclear carboxylate-based cluster  $[\text{Tb}_9(\mu_3\text{O})_2(\mu_3\text{-OH})_{12}(\text{H}_2\text{O})_9(\text{O}_2\text{C}-)_{12}]^-$  is formed and it has a two-fold disorder with equal occupancy (Fig. S4†). In each  $\text{Tb}_9$  cluster, nine  $\text{Tb}^{3+}$  ions are arranged in a tricapped trigonal prism (Fig. S5†): six  $\text{Tb}^{3+}$  ions are 8-coordinated with two carboxylate groups from individual  $\text{TCPE}^{4-}$  ligands, four  $\mu_3\text{-OH}$ , one  $\mu_3\text{O}$ , and one terminal water ligand in a distorted bicapped trigonal prismatic geometry (Fig. S6a†), while the other three coordinate to four carboxylates of four  $\text{TCPE}^{4-}$  ligands, four  $\mu_3\text{-OH}$ , and one apical water molecule, showing a distorted tricapped trigonal prism geometry (Fig. S6b†). From a topological viewpoint, the hexagonal prismatic  $\text{Tb}_9$  cluster (Fig. 1b) and the rectangular  $\text{TCPE}^{4-}$  ligand (Fig. 1a) serve as a 12-connected (12-c) and 4-c node to yield a (4,12)-c **shp** net (Fig. 1d). The resulting highly connected framework features a high density of aromatic rings from  $\text{TCPE}^{4-}$ , constituting a large  $\pi$ -conjugated pore surface and encompassing three types of one-dimensional (1D) channels. Among them, the largest channel A has a triangular aperture with an equilateral side length of 9.5 Å running along the *c*-axis (Fig. 1c), while the rhombus channel B and the isosceles triangular channel C are elongated along both the *a*- and *b*-axis, with the pore diameters of 7.0 and 4.5 Å, respectively (Fig. 1e and f). The total guest-accessible volume calculated using PLATON is 35.3% of the unit-cell volume, affording enough space for gas accommodation.

The phase purity of the as-synthesized sample was verified by comparing the experimental powder X-ray diffraction (PXRD) pattern to the simulation result. Immersing the

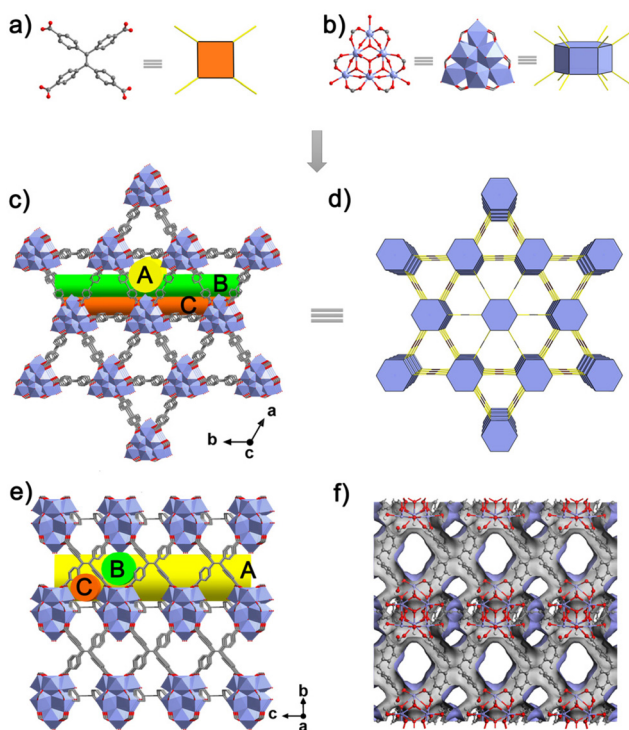


**Fig. 1** (a and b) The 4-c TCPE<sup>4-</sup> ligand and the 12-c nonanuclear Tb<sub>9</sub> cluster. (c and e) The 3D framework of NKU-200-Tb with three types of 1D channels along the *c*- and *a*-axis, respectively. (d) The topological simplification of the (4,12)-c shp net. (f) View of channels B and C in the Connolly surface.

sample in a series of organic solvents and aqueous solutions with a broad pH range of 3–12 for 24 h gave no indication of decomposition or crystallinity loss in PXRD profiles (Fig. S7 and S8†), suggesting its great chemical stability. Thermogravimetric (TG) analysis further reveals that the framework does not decompose until 500 °C (Fig. S9†), also supported by the variable-temperature (VT) PXRD data (Fig. S10†). Thus, the excellent structural stability of NKU-200-Tb under harsh thermal and chemical conditions places it among the most stable C<sub>2</sub>H<sub>6</sub>-selective MOFs reported in the literature (Table S2†), which should be attributed to not only the high connectivity of the framework, but also the strong coordination bond between the Tb<sup>3+</sup> ion and carboxylate oxygen atom, according to the concept of hard and soft acids and bases (HSAB).<sup>25</sup> In order to investigate the permanent porosity of NKU-200-Tb, the sample was then subjected to methanol exchange and dynamic vacuum activation at 150 °C for 12 h. The unchanged PXRD curve confirms again the retention of its structural integrity and crystallinity after desolvation (Fig. S7†). The N<sub>2</sub> adsorption–desorption experiment on NKU-200-Tb at 77 K shows a reversible type-I isotherm (Fig. S11†), indicative of its microporous characteristic. The corresponding Brunauer–Emmett–Teller (BET) surface area and the total pore volume are then determined to be 792.7 m<sup>2</sup> g<sup>-1</sup> and 0.32 cm<sup>3</sup> g<sup>-1</sup> (calculated by a single point method at  $P/P_0 = 0.90$ ), respectively, very close to the theoretical pore volume value of

0.35 cm<sup>3</sup> g<sup>-1</sup> derived from single-crystal structural analysis. The estimated pore size distribution using nonlocal density functional theory lies in the range of 7–10 Å (Fig. S11†), also in agreement with the crystallographic data. The high structural stability and porosity of NKU-200-Tb, also proved by the N<sub>2</sub> adsorption curves after harsh treatments (Fig. S12†), pave the way for gas adsorptive separation.

The single-component adsorption isotherms of NKU-200-Tb for C<sub>2</sub>H<sub>6</sub> and C<sub>2</sub>H<sub>4</sub> were measured at 273 and 298 K, respectively. As shown in Fig. 2a and b, this Tb-MOF exhibits the desirable adsorption preference for C<sub>2</sub>H<sub>6</sub> over C<sub>2</sub>H<sub>4</sub> at both temperatures and throughout the whole pressure region, fulfilling the demand for one-step C<sub>2</sub>H<sub>4</sub> purification from binary C<sub>2</sub>H<sub>6</sub>/C<sub>2</sub>H<sub>4</sub> mixtures. At 298 K and 1 bar, the adsorption uptake of C<sub>2</sub>H<sub>6</sub> on NKU-200-Tb reaches up to 60.27 cm<sup>3</sup> g<sup>-1</sup> (2.69 mmol g<sup>-1</sup>), much higher than that of C<sub>2</sub>H<sub>4</sub> (39.95 cm<sup>3</sup> g<sup>-1</sup>, 1.78 mmol g<sup>-1</sup>) with a large uptake ratio of 151%, surpassing many leading C<sub>2</sub>H<sub>6</sub>-selective MOFs (Table S3†). We envisioned that the adsorption affinity order of C<sub>2</sub>H<sub>6</sub> > C<sub>2</sub>H<sub>4</sub> on NKU-200-Tb is a consequence of its nonpolar/hydrophobic pore surface. To validate the pore surface polarity, we also collected the CO<sub>2</sub> and water vapor adsorption isotherms at 298 K. As seen from Fig. S13,† the CO<sub>2</sub> uptake increases slowly and constantly over the whole pressure range and reaches 32.99 cm<sup>3</sup> g<sup>-1</sup> (1.47 mmol g<sup>-1</sup>) at 1 bar, much lower than that

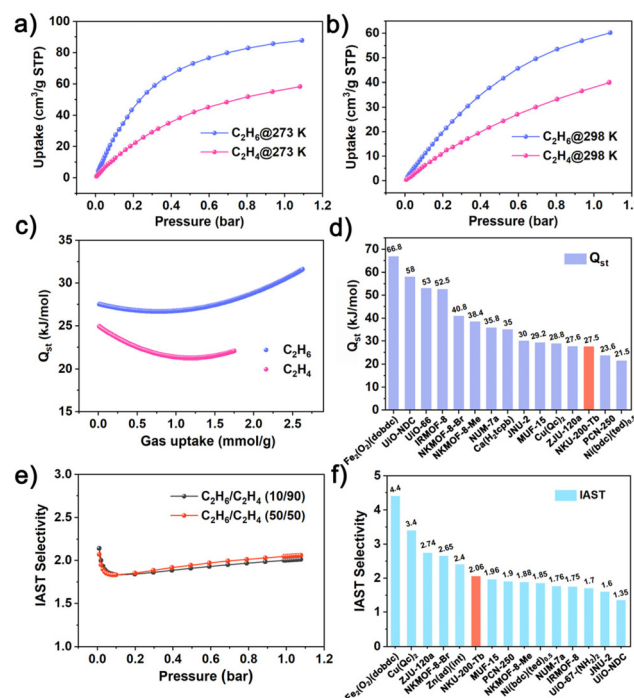


**Fig. 2** (a and b) The adsorption isotherms for C<sub>2</sub>H<sub>6</sub> and C<sub>2</sub>H<sub>4</sub> on NKU-200-Tb at 273 and 298 K, respectively. (c) The coverage-dependent  $Q_{st}$  curves of C<sub>2</sub>H<sub>6</sub> and C<sub>2</sub>H<sub>4</sub>. (d) Comparison of the zero-coverage  $Q_{st}$  of C<sub>2</sub>H<sub>6</sub> with those of some representative C<sub>2</sub>H<sub>6</sub>-selective MOFs. (e) IAST selectivities for C<sub>2</sub>H<sub>6</sub>/C<sub>2</sub>H<sub>4</sub> (50/50 and 10/90, v/v) mixtures at 298 K and 1 bar. (f) Comparison of the C<sub>2</sub>H<sub>6</sub>/C<sub>2</sub>H<sub>4</sub> (50/50, v/v) selectivity at 298 K and 1 bar with those of top-performing C<sub>2</sub>H<sub>6</sub>-selective MOFs.

of  $\text{C}_2\text{H}_6$ , excluding the presence of open metal sites that have high affinity for  $\text{CO}_2$ .<sup>26,27</sup> As for water vapor, the adsorption-desorption isotherm displays a typical S-shaped curve with a hysteresis loop and an inflection point at a relatively high moisture level (Fig. S14†). This result indicates a low binding affinity toward  $\text{H}_2\text{O}$  and manifests the hydrophobicity of the inner pore surface of **NKU-200-Tb**,<sup>16,28,29</sup> in line with the presence of abundant aromatic rings in this system.

To quantitatively assess the binding affinities of **NKU-200-Tb** toward  $\text{C}_2\text{H}_6$  and  $\text{C}_2\text{H}_4$ , we calculated the isosteric enthalpy of adsorption ( $Q_{\text{st}}$ ) using the virial equation based on the isotherms at 273 and 298 K (Fig. S15, S16 and Table S4†). The estimated zero-coverage  $Q_{\text{st}}$  for  $\text{C}_2\text{H}_6$  is  $27.54 \text{ kJ mol}^{-1}$ , higher than the value of  $24.93 \text{ kJ mol}^{-1}$  for  $\text{C}_2\text{H}_4$  (Fig. 2c), thus reflecting a binding affinity order of  $\text{C}_2\text{H}_6 > \text{C}_2\text{H}_4$  on **NKU-200-Tb** consistent with the inverse adsorption isotherms (Fig. 2a and b). Besides that, the coverage-dependent  $Q_{\text{st}}$  curve of  $\text{C}_2\text{H}_6$  displays an overall ascending trend, indicative of favorable adsorbate-adsorbate interactions at higher loadings,<sup>30,31</sup> whereas that of  $\text{C}_2\text{H}_4$  shows an apparent descending trend in the initial coverage range. Such an enlarged discrepancy in  $Q_{\text{st}}$  values also benefits the challenging  $\text{C}_2\text{H}_6/\text{C}_2\text{H}_4$  separation. Noteworthily, the zero-coverage  $Q_{\text{st}}$  of  $\text{C}_2\text{H}_6$  on **NKU-200-Tb** is significantly lower than those of many benchmark  $\text{C}_2\text{H}_6$ -selective MOFs (Fig. 2d), including NCMOF-Br/-Me ( $40.8/38.4 \text{ kJ mol}^{-1}$ ),<sup>14</sup>  $\text{Fe}_2\text{O}_2(\text{dobdc})$  ( $66.8 \text{ kJ mol}^{-1}$ ),<sup>15</sup> IR-MOF-8 ( $52.5 \text{ kJ mol}^{-1}$ ),<sup>20</sup> and  $\text{UiO-66}$  ( $53 \text{ kJ mol}^{-1}$ ).<sup>32</sup> The comparatively low  $Q_{\text{st}}$  value will facilitate the regeneration of **NKU-200-Tb** by avoiding harsh treatments and high energy consumption.

In order to evaluate the separation ability of **NKU-200-Tb**, we employed the ideal adsorbed solution theory (IAST) to estimate the adsorption selectivities for  $\text{C}_2\text{H}_6/\text{C}_2\text{H}_4$  mixtures with different composition ratios. By fitting the isotherms according to the dual-site Langmuir-Freundlich equation (Fig. S17 and S18†), the  $\text{C}_2\text{H}_6/\text{C}_2\text{H}_4$  (50/50 and 10/90, v/v) selectivities are calculated to be 2.06 and 2.01, respectively, at 298 K and 1 bar (Fig. 2e). It is worth noting that the  $\text{C}_2\text{H}_6/\text{C}_2\text{H}_4$  (50/50, v/v) selectivity on **NKU-200-Tb** (2.06) is superior or comparable to those of most top-performing  $\text{C}_2\text{H}_6$ -selective adsorbents (Fig. 2f and Table S3†), such as PCN-250 (1.9),<sup>33</sup> JNU-2 (1.6),<sup>34</sup>  $\text{Ni}(\text{bdc})(\text{ted})_{0.5}$  (1.85),<sup>35</sup>  $\text{UiO-67-(NH}_2)_2$  (1.7),<sup>36</sup> and  $\text{Zn}(\text{ad})(\text{int})$  (2.4),<sup>37</sup> and only significantly lower than those of NCMOF-Br (2.65),<sup>14</sup>  $\text{Fe}_2(\text{O}_2)(\text{dobdc})$  (4.4),<sup>15</sup> ZJU-120a (2.74),<sup>21</sup> and  $\text{Cu}(\text{Qc})$  (3.4).<sup>22</sup>

Such a high  $\text{C}_2\text{H}_6/\text{C}_2\text{H}_4$  selectivity on **NKU-200-Tb** inspired us to further explore its actual separation performance. Fixed-bed dynamic breakthrough experiments were then performed at 298 K and 1 bar, with a total inlet flow rate of  $10.0 \text{ mL min}^{-1}$  by using He as the carrier gas (50%, vol%). When a  $\text{C}_2\text{H}_6/\text{C}_2\text{H}_4$  gas mixture of an industrially relevant composition (10/90, v/v) was passed through the packed column of activated **NKU-200-Tb**,  $\text{C}_2\text{H}_4$  was first eluted from the outlet at 314 s and quickly reached saturation, whereas the  $\text{C}_2\text{H}_6$  impurity was still retained in the column for an additional time of 104 s, during which the  $\text{C}_2\text{H}_4$  gas with high purity (>99.9%) can be directly harvested (Fig. 3a). The breakthrough experiments

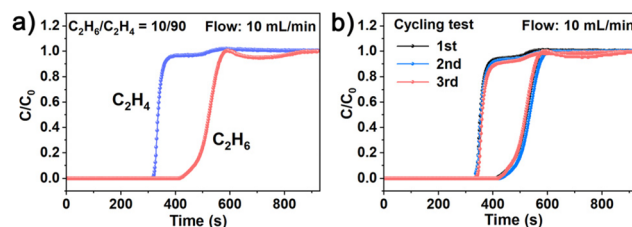
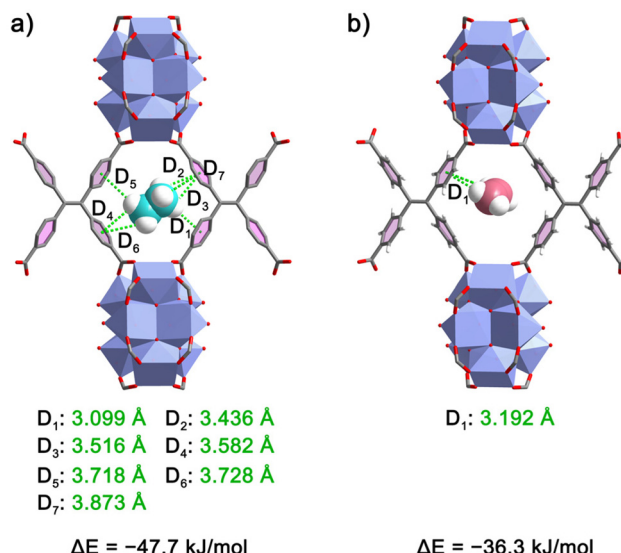


Fig. 3 (a) Dynamic breakthrough curves for a binary  $\text{C}_2\text{H}_6/\text{C}_2\text{H}_4$  (10/90, v/v) mixture. (b) Cyclic breakthrough tests under the same conditions. All the breakthrough experiments were performed at 298 K and 1 bar, with a total flow rate of  $10 \text{ mL min}^{-1}$  using He as the carrier gas (50%, vol%).

prove that **NKU-200-Tb** is capable of separating pure  $\text{C}_2\text{H}_4$  from a low-level of  $\text{C}_2\text{H}_6$  through one-step adsorption without resorting to energy-intensive desorption steps. We also conducted the breakthrough experiments for an equimolar  $\text{C}_2\text{H}_6/\text{C}_2\text{H}_4$  mixture and the results demonstrate that this MOF can also achieve one-step  $\text{C}_2\text{H}_4$  purification from mixtures with high concentrations of  $\text{C}_2\text{H}_6$  (Fig. S19†). For industrial applications, the stability and recyclability of an adsorbent are also important. Cyclic breakthrough tests confirm that its separation performance could be well preserved for three continuous cycles without noticeable deterioration in retention time (Fig. 3b), wherein the adsorbent was easily regenerated by heating at  $150^\circ\text{C}$  under He flow for 5 h after each cycle.

To gain insight into the preferential adsorption of  $\text{C}_2\text{H}_6$  over  $\text{C}_2\text{H}_4$  on **NKU-200-Tb** at the molecular level, we performed DFT calculations to unveil the preferred adsorption sites and gas-framework interactions. The optimization results reveal that the most favorable trapping site for both  $\text{C}_2\text{H}_6$  and  $\text{C}_2\text{H}_4$  is situated at the rhombus aperture window of channel B (*i.e.*, on the pore wall of channel A) encompassed by two  $\text{Tb}_9$  clusters and two  $\text{TCPE}^{4-}$  ligands (Fig. 1e), which can be conceived of as a nanotrap ( $7.0 \text{ \AA}$ ) possessing dense aromatic rings and suitable size for  $\text{C}_2\text{H}_6/\text{C}_2\text{H}_4$  separation.<sup>38</sup> Within this confined space, the two  $\text{C}_2$  hydrocarbon molecules adopt distinct positions and orientations (Fig. 4). With a larger vdW surface area and more C-H binding sites,  $\text{C}_2\text{H}_6$  is grasped at the nanotrap center with an orientation perpendicular to channel B. In contrast,  $\text{C}_2\text{H}_4$  is located close to only one side of the aperture and oriented parallel to the *a*-*b*-axis in channel B. As a result, one  $\text{C}_2\text{H}_6$  molecule forms seven C-H $\cdots\pi$  ( $3.099\text{--}3.873 \text{ \AA}$ ) interactions with all four neighboring phenyl rings from two  $\text{TCPE}^{4-}$  ligands, giving a static binding energy of  $-47.7 \text{ kJ mol}^{-1}$  (Fig. 4a), while one  $\text{C}_2\text{H}_4$  molecule is in contact with only one phenyl ring *via* one C-H $\cdots\pi$  ( $3.192 \text{ \AA}$ ) bond with a lower binding energy of  $-36.3 \text{ kJ mol}^{-1}$  (Fig. 4b). Clearly, the differences in the number and distance of C-H $\cdots\pi$  interactions account for the preferential adsorption of  $\text{C}_2\text{H}_6$  over  $\text{C}_2\text{H}_4$  and the discrepancy between the static binding energies also explains the binding affinity order of  $\text{C}_2\text{H}_6 > \text{C}_2\text{H}_4$  manifested in the  $Q_{\text{st}}$ . The calculation results not only show the effectiveness of promoting the density of aromatic rings to enhance



**Fig. 4** (a and b) Predicted adsorption sites, interactions, and binding energies ( $\Delta E$ ) of  $\text{C}_2\text{H}_6$  and  $\text{C}_2\text{H}_4$  in the nanotrap of **NKU-200-Tb** obtained from the DFT optimization. The green dashed lines refer to  $\text{C}-\text{H}\cdots\pi$  interactions.

$\text{C}_2\text{H}_6$  trapping and recognition ability, but also signify the synergy with pore space confinement.

In summary, a highly connected Tb-MOF (**NKU-200-Tb**) was employed to implement one-step  $\text{C}_2\text{H}_4$  purification. Based on the reticular assembly of a nonanuclear  $\text{Tb}_9$  cluster and the aromatic ligand  $\text{TCPE}^{4-}$ , the resulting MOF not only exhibits great thermal and chemical stability, but also possesses an inert/hydrophobic pore surface composed of dense nonpolar aromatic rings. As a result, **NKU-200-Tb** shows a higher adsorption capacity for  $\text{C}_2\text{H}_6$  ( $60.27 \text{ cm}^3 \text{ g}^{-1}$ ) than for  $\text{C}_2\text{H}_4$  ( $39.95 \text{ cm}^3 \text{ g}^{-1}$ ) at 298 K and 1 bar, highlighted with an uptake ratio of up to 151% and an excellent inverse  $\text{C}_2\text{H}_6/\text{C}_2\text{H}_4$  selectivity of 2.06, surpassing many leading  $\text{C}_2\text{H}_6$ -selective MOFs. Further DFT calculations disclose that two  $\text{Tb}_9$  clusters and two  $\text{TCPE}^{4-}$  ligands constitute a specific size-matching nanotrap to promote the  $\text{C}_2\text{H}_6$  adsorption by providing abundant  $\text{C}-\text{H}\cdots\pi$  interactions within a confined pore space. With the above advantages, this MOF realizes the desirable one-step acquisition of polymer-grade  $\text{C}_2\text{H}_4$  ( $>99.9\%$ ) from a binary  $\text{C}_2\text{H}_6/\text{C}_2\text{H}_4$  (10/90, v/v) gas mixture with good recyclability, as demonstrated by breakthrough experiments. Our work not only reports a new example of one-step  $\text{C}_2\text{H}_4$  purification adsorbents, but importantly also sheds new light on the design of paraffin-selective MOFs in terms of the engineering of inert/nonpolar pore surfaces with an enhanced confinement effect.

## Author contributions

Jing-Jing Pang: investigation, visualization, data curation, and writing – original draft. Zhi-Han Ma, Qiang-Qiang Yang, Kuo

Zhang, and Xin Lian: data curation. Hongliang Huang and Zhao-Quan Yao: formal analysis, conceptualization, and supervision. Baiyan Li: validation. Jian Xu: supervision, conceptualization, writing – review & editing, and funding acquisition. Xian-He Bu: resources.

## Conflicts of interest

There are no conflicts to declare.

## Acknowledgements

This work was supported by the National Natural Science Foundation of China (22171144 and 22001132) and the Fundamental Research Funds for the Central Universities (Nankai University). The authors would like to thank Shiyanjia Lab (<https://www.shiyanjia.com>) for the crystallographic analysis.

## Notes and references

1. I. Amghizar, L. A. Vandewalle, K. M. Van Geem and G. B. Marin, New trends in olefin production, *Engineering*, 2017, **3**, 171–178.
2. J. R. Li, R. J. Kuppler and H. C. Zhou, Selective gas adsorption and separation in metal–organic frameworks, *Chem. Soc. Rev.*, 2009, **38**, 1477–1504.
3. T. Ren, M. Patel and K. Blok, Olefins from conventional and heavy feedstocks: energy use in steam cracking and alternative processes, *Energy*, 2006, **31**, 425–451.
4. D. S. Sholl and R. P. Lively, Seven chemical separations to change the world, *Nature*, 2016, **532**, 435–437.
5. W. D. Fan, X. R. Zhang, Z. X. Kang, X. P. Liu and D. F. Sun, Isoreticular chemistry within metal–organic frameworks for gas storage and separation, *Coord. Chem. Rev.*, 2021, **440**, 213968.
6. L. F. Yang, S. H. Qian, X. B. Wang, X. L. Cui, B. L. Chen and H. B. Xing, Energy-efficient separation alternatives: metal–organic frameworks and membranes for hydrocarbon separation, *Chem. Soc. Rev.*, 2020, **49**, 5359–5406.
7. H. Furukawa, K. E. Cordova, M. O’Keeffe and O. M. Yaghi, The chemistry and applications of metal–organic frameworks, *Science*, 2013, **341**, 1230444.
8. R. B. Lin, Z. J. Zhang and B. L. Chen, Achieving high performance metal–organic framework materials through pore engineering, *Acc. Chem. Res.*, 2021, **54**, 3362–3376.
9. R. B. Lin, L. B. Li, H. L. Zhou, H. Wu, C. H. He, S. Li, R. Krishna, J. P. Li, W. Zhou and B. L. Chen, Molecular sieving of ethylene from ethane using a rigid metal–organic framework, *Nat. Mater.*, 2016, **17**, 1128–1133.
10. M. Xie, Z. Lu, W. G. Lu and D. Li, Kinetic separation of  $\text{C}_2\text{H}_6/\text{C}_2\text{H}_4$  in a cage-interconnected metal–organic framework: an interaction-screening mechanism, *Inorg. Chem. Front.*, 2022, **9**, 2697–2705.

11 B. Li, Y. Zhang, R. Krishna, K. Yao, Y. Han, Z. Wu, D. Ma, Z. Shi, T. Pham, B. Space, J. Liu, P. K. Thallapally, J. Liu, M. Chrzanowski and S. Ma, Introduction of  $\pi$ -complexation into porous aromatic framework for highly selective adsorption of ethylene over ethane, *J. Am. Chem. Soc.*, 2014, **136**, 8654–8660.

12 E. D. Bloch, W. L. Queen, R. Krishna, J. M. Zadrozny, C. M. Brown and J. R. Long, Hydrocarbon separations in a metal–organic framework with open iron(II) coordination sites, *Science*, 2012, **335**, 1606–1610.

13 D. F. Lv, P. J. Zhou, J. H. Xu, S. Tu, F. Xu, J. Yan, H. X. Xi, W. B. Yuan, Q. Fu, X. Chen and Q. B. Xia, Recent advances in adsorptive separation of ethane and ethylene by  $C_2H_6$ -selective MOFs and other adsorbents, *Chem. Eng. J.*, 2022, **431**, 133208.

14 S. B. Geng, E. Lin, X. Li, W. S. Liu, T. Wang, Z. F. Wang, D. Sensharma, S. Darwish, Y. H. Andaloussi, T. Pham, P. Cheng, M. J. Zaworotko, Y. Chen and Z. J. Zhang, Scalable room-temperature synthesis of highly robust ethane-selective metal–organic frameworks for efficient ethylene purification, *J. Am. Chem. Soc.*, 2021, **143**, 8654–8660.

15 L. B. Li, R. B. Lin, R. Krishna, H. Li, S. C. Xiang, H. Wu, J. P. Li, W. Zhou and B. L. Chen, Ethane/ethylene separation in a metal–organic framework with iron-peroxo sites, *Science*, 2018, **362**, 443–446.

16 S. S. Jiang, L. D. Guo, L. H. Chen, C. H. Song, B. J. Liu, Q. W. Yang, Z. G. Zhang, Y. W. Yang, Q. L. Ren and Z. B. Bao, A strongly hydrophobic ethane-selective metal–organic framework for efficient ethane/ethylene separation, *Chem. Eng. J.*, 2022, **442**, 136152.

17 W. S. Liu, S. B. Geng, N. Li, S. Wang, S. P. Jia, F. Z. Jin, T. Wang, K. A. Forrest, T. Pham, P. Cheng, Y. Chen, J. G. Ma and Z. J. Zhang, Highly robust microporous metal–organic frameworks for efficient ethylene purification under dry and humid conditions, *Angew. Chem., Int. Ed.*, 2023, **62**, e202217662.

18 S. Q. Yang and T. L. Hu, Reverse-selective metal–organic framework materials for the efficient separation and purification of light hydrocarbons, *Coord. Chem. Rev.*, 2022, **468**, 214628.

19 Z. Y. Di, C. P. Liu, J. D. Pang, S. X. Zou, Z. Y. Ji, F. L. Hu, C. Chen, D. Q. Yuan, M. C. Hong and M. Y. Wu, A metal–organic framework with nonpolar pore surfaces for the one-step acquisition of  $C_2H_4$  from a  $C_2H_4$  and  $C_2H_6$  mixture, *Angew. Chem., Int. Ed.*, 2022, **61**, e202210343.

20 J. Pires, M. L. Pinto and V. K. Saini, Ethane selective IRMOF-8 and its significance in ethane–ethylene separation by adsorption, *ACS Appl. Mater. Interfaces*, 2014, **6**, 12093–12099.

21 J. Y. Pei, J. X. Wang, K. Shao, Y. Yang, Y. J. Cui, H. Wu, W. Zhou, B. Li and G. D. Qian, Engineering microporous ethane-trapping metal–organic frameworks for boosting ethane/ethylene separation, *J. Mater. Chem. A*, 2020, **8**, 3613–3620.

22 R. B. Lin, H. Wu, L. B. Li, X. L. Tang, Z. Q. Li, J. K. Gao, H. Cui, W. Zhou and B. L. Chen, Boosting ethane/ethylene separation within isoreticular ultramicroporous metal–organic frameworks, *J. Am. Chem. Soc.*, 2018, **140**, 12940–12946.

23 O. T. Qazvini, R. Babarao, Z. L. Shi, Y. B. Zhang and S. G. Telfer, A robust ethane-trapping metal–organic framework with a high capacity for ethylene purification, *J. Am. Chem. Soc.*, 2019, **141**, 5014–5020.

24 J. J. Pang, Z. Q. Yao, K. Zhang, Q. W. Li, Z. X. Fu, R. Zheng, W. Li, J. Xu and X. H. Bu, Real-time in situ volatile organic compound sensing by a dual-emissive polynuclear  $Ln$ -MOF with pronounced  $Ln^{III}$  luminescence response, *Angew. Chem., Int. Ed.*, 2023, **62**, e202217456.

25 L. Feng, K. Y. Wang, G. S. Day, M. R. Ryder and H. C. Zhou, Destruction of metal–organic frameworks: positive and negative aspects of stability and lability, *Chem. Rev.*, 2020, **120**, 13087–13133.

26 X. Ye, S. K. Xian, H. Cui, K. Tan, L. S. Gong, B. Liang, T. Pham, H. Pandey, R. Krishna, P. C. Lan, K. A. Forrest, B. Space, T. Thonhauser, J. Li and S. Q. Ma, Metal–organic framework based hydrogen-bonding nanotrap for efficient acetylene storage and separation, *J. Am. Chem. Soc.*, 2022, **144**, 1681–1689.

27 Z. Y. Di, C. P. Liu, J. D. Pang, C. Chen, F. L. Hu, D. Q. Yuan, M. Y. Wu and M. C. Hong, Cage-like porous materials with simultaneous high  $C_2H_2$  storage and excellent  $C_2H_2/CO_2$  separation performance, *Angew. Chem., Int. Ed.*, 2021, **60**, 10828–10832.

28 H. Furukawa, F. Gándara, Y. B. Zhang, J. C. Jiang, W. L. Queen, M. R. Hudson and O. M. Yaghi, Water adsorption in porous metal–organic frameworks and related materials, *J. Am. Chem. Soc.*, 2014, **136**, 4369–4381.

29 G. D. Wang, Y. Z. Li, W. J. Shi, L. Hou, Y. Y. Wang and Z. H. Zhu, One-step  $C_2H_4$  purification from ternary  $C_2H_6/C_2H_4/C_2H_2$  mixtures by a robust metal–organic framework with customized pore environment, *Angew. Chem., Int. Ed.*, 2022, **61**, e202205427.

30 P. Q. Liao, W. X. Zhang, J. P. Zhang and X. M. Chen, Efficient purification of ethene by an ethane-trapping metal–organic framework, *Nat. Commun.*, 2015, **6**, 8697–8705.

31 B. Y. Zhu, J. W. Cao, S. Mukherjee, T. Pham, T. Zhang, T. Wang, X. Jiang, K. A. Forrest, M. J. Zaworotko and K. J. Chen, Pore engineering for one-step ethylene purification from a three-component hydrocarbon mixture, *J. Am. Chem. Soc.*, 2021, **143**, 1485–1492.

32 J. Pires, J. Fernandes, K. Dedecker, J. R. B. Gomes, G. Pérez-Sánchez, F. Nouar, C. Serre and M. L. Pinto, Enhancement of ethane selectivity in ethane–ethylene mixtures by perfluoro groups in Zr-based metal–organic frameworks, *ACS Appl. Mater. Interfaces*, 2019, **11**, 27410–27421.

33 Y. W. Chen, Z. W. Qiao, H. X. Wu, D. F. Lv, R. F. Shi, Q. B. Xia, J. Zhou and Z. Li, An ethane-trapping MOF PCN-250 for highly selective adsorption of ethane over ethylene, *Chem. Eng. Sci.*, 2018, **175**, 110–117.

34 H. Zeng, X. J. Xie, M. Xie, Y. L. Huang, D. Luo, T. Wang, Y. F. Zhao, W. G. Lu and D. Li, Cage-interconnected metal-organic framework with tailored apertures for efficient  $C_2H_6/C_2H_4$  separation under humid conditions, *J. Am. Chem. Soc.*, 2019, **141**, 20390–20396.

35 W. Liang, F. Xu, X. Zhou, J. Xiao, Q. Xia, Y. Li and Z. Li, Ethane selective adsorbent  $Ni(bdc)(ted)_{0.5}$  with high uptake and its significance in adsorption separation of ethane and ethylene, *Chem. Eng. Sci.*, 2016, **148**, 275–281.

36 X. W. Gu, J. X. Wang, E. Y. Wu, H. Wu, W. Zhou, G. D. Qian, B. L. Chen and B. Li, Immobilization of Lewis basic sites into a stable ethane-selective MOF enabling one-step separation of ethylene from a ternary mixture, *J. Am. Chem. Soc.*, 2022, **144**, 2614–2623.

37 Q. Ding, Z. Q. Zhang, Y. L. Liu, K. G. Chai, R. Krishna and S. Zhang, One-step ethylene purification from ternary mixtures in a metal–organic framework with customized pore chemistry and shape, *Angew. Chem., Int. Ed.*, 2022, **61**, e202208134.

38 J. Q. Liu, K. Zhou, S. Ullah, J. F. Miao, H. Wang, T. Thonhauser and J. Li, Precise pore engineering of fcu-type Y-MOFs for one-step  $C_2H_4$  purification from ternary  $C_2H_6/C_2H_4/C_2H_2$  mixtures, *Small*, 2023, 2304460.